Wave Structures in Simulated 25 mm Rotating Detonation Rocket Engine

Mathias C. Ross & Jason R. Burr
U.S. Air Force Research Laboratory
Edwards, CA, USA

1 Introduction

Rotating detonation technology may enable the development of efficient combustors in a small form factor, but it is not yet known how much that form factor affects the wave structure inside such devices. A study by Knowlen et al. [1] demonstrated that it is possible to scale a rotating detonation rocket engine (RDRE) to an outer diameter of 25.4 mm and still observe frequency content in the chamber. This work builds on that prior study by conducting large eddy simulations (LES) of the 25.4 mm engine, enabling a look at details in the internal flow field. Additionally, the design by Knowlen et al. [1] is a scaled version of a much-studied 76.2 mm design [2], and existing simulations of that engine can be compared to these results of the smaller version [3, 4].

2 Simulation Methodology and Case Setup

Simulations were conducted using the in-house Combustion Engineering LES Technology (CELESTE) solver, which is derived from the LES with Linear Eddy (LESLIE) code [5]. A second-order MacCormack finite-volume scheme was used as the primary central scheme [6] with a third-order monotonic upstream-centered scheme for conservation laws (MUSCL) approach implemented for shock capturing [7]. Turbulence was accounted for using an additional transport equation for the sub-grid kinetic

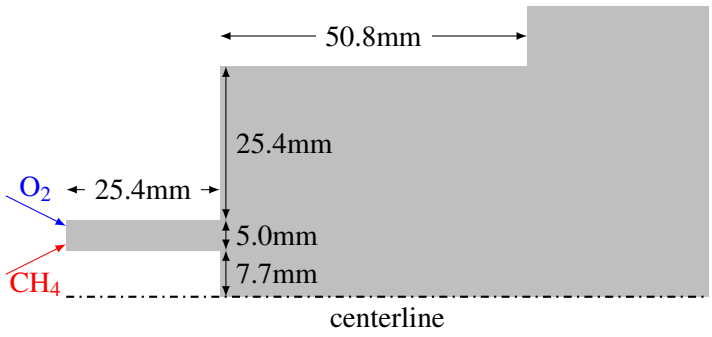

Figure 1: Simplified simulation geometry.

Correspondence to: mathias.ross.1@us.af.mil

Table 1: Inflow conditions for the three simulations.

	Case 1	Case 2	Case 3
ϕ	1.14	0.46	0.43
$\dot{m}$, g/s	76.5	75.2	127.0

energy, k_{sgs} [8]. Chemistry was modeled using FFCMy-12, which is a finite-rate model with 12 species and 38 reactions [9]. For more details on the numerical setup see Lietz et al. [10].

The simulation domain matched the experimental setup at the University of Washington which was used to test the 25 mm RDRE [1], including injector geometry and experimental dump tank; a simplified representation is shown in Fig. 1. The engine itself was designed to be a scaled-down version of the 76.2 mm American Institute of Aeronautics and Astronautics (AIAA) Model Validation for Propulsion (MVP) geometry [2]. A structured hexahedral mesh was constructed to target a cell width of 50 $\mu\mathrm{m}$ near injection, and totalled 25 M cells. Engine walls were modeled using adiabatic, no-slip conditions. Three simulations were conducted, at varying overall equivalence ratios and mass flow rates; conditions are listed in Table 1.

3 Results

Table 2: Comparing simulation results to experimental measurements. CTAP measurements taken 17 mm from injection; simulation CTAP values are time-averaged pressures. Wavespeed of dominant direction given for case 1.

	Case 1		Case 2		Case 3	
	Exp.	Sim.	Exp.	Sim.	Exp.	Sim.
No. of waves	1/1	1/1	1	1	1	1
Wave speed, m/s	1256	837	1324	1228	1427	1256
CTAP, MPa	0.32	0.35	0.23	0.24	0.37	0.41

A summary comparing the simulations results to experiment is presented in Table 2. All three simulations established quasi-periodic behavior within 1 ms of simulation initialization, with pressure waves traveling azimuthally inside the 25 mm annulus. Case 1 developed counter-propagating waves, with one wave structure traveling in each azimuthal direction. Counter-propagating behavior was also observed experimentally for this condition [1]. The other two cases, operating in the fuel-lean regime, developed a wave traveling in only one direction, which again matches experimental observations.

Average wave speeds in Table 2 are calculated assuming the radius in the center of the channel. Case 1 operated with a higher average pressure than case 2, but a lower wave speed – even though the overall equivalence ratio would suggest case 1 could operate at a higher Chapman-Jouguet velocity. Taken together, this indicates that less of the potential reactant energy was coupled to the pressure structures, a conclusion which is borne out by an investigation of the flow composition: in case 1, the engine exhaust had an unburnt methane mass fraction of 0.045, while the other two cases had negligible amounts of unburnt methane in the exhaust. The flow conditions of case 1 were chosen to match mass flux and equivalence ratios of a well-validated 76.2 mm version of this engine, which operated with two co-rotating waves traveling at 1613 m/s [2, 4]. This is a situation where scaling the engine changed the internal dynamics, worsening the performance of the engine by reducing an overall combustion efficiency.

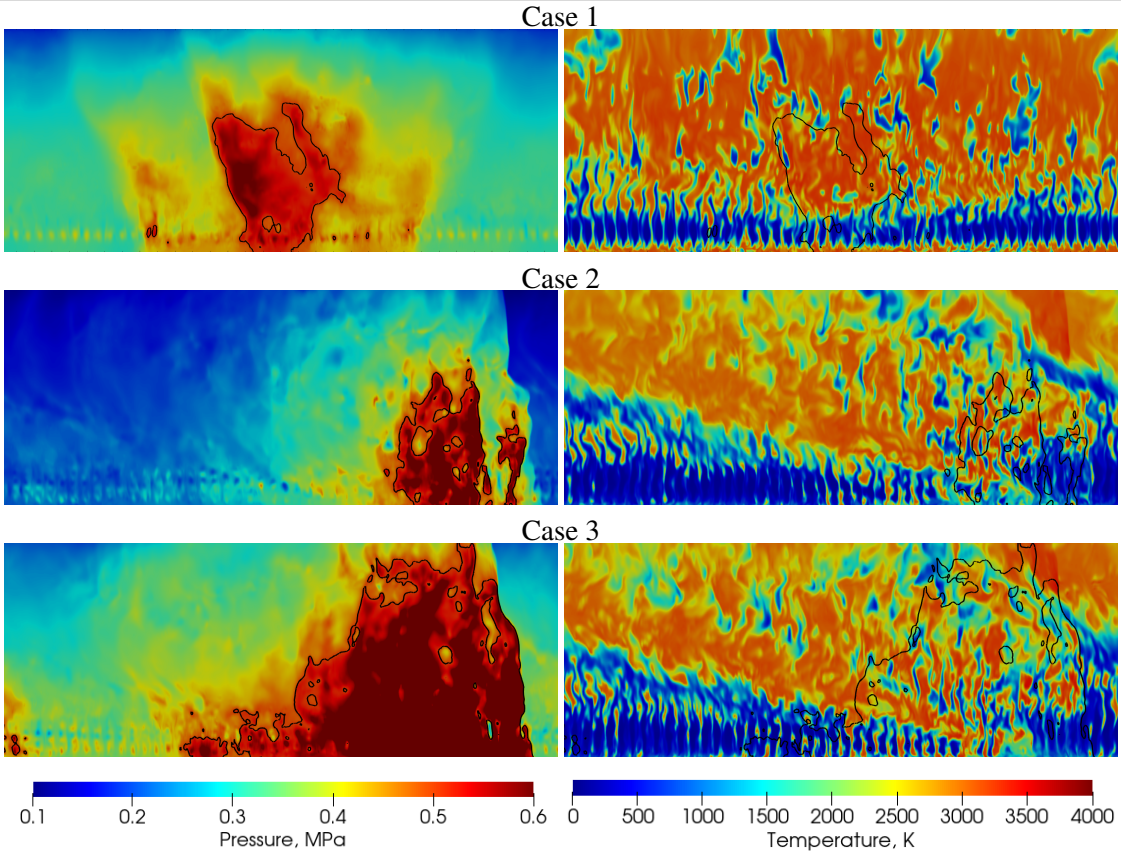

Figure 2: Channel-center snapshots for the three simulations, showing pressure (left) and temperature (right). Black isocontour denotes 0.5 MPa.

Snapshots of the unwrapped center of the channel are shown in Fig. 2 for the three simulations. Each wave exhibited a double-shock structure, with two high-pressure regions traveling in the same direction, but with a small separation; in Fig. 2, this double-shock phenomenon is most clearly visible in the pressure field of case 2. Similar behavior has been observed in simulations of the 76.2 mm predecessor to this geometry [3, 4]. It can be seen by inspection of the temperature field that the majority of the heat release occured after the passage of the second pressure structure.

The same instants in time shown from Fig. 2 are shown in Fig. 3 from a different perspective. Figure 2 shows the temperature field for planes normal to the annular axis, with 6 mm separating each plane. In order from top to bottom, the five planes shown are 25 mm, 19 mm, 13 mm, 7 mm, and 1 mm from injection. An examination of the axis-normal temperature fields reveal a radial stratification throughout the chamber, and in all three simulations. Case 1 developed a layer of cold reactants on the inner wall, which contained both methane and oxygen; counter-intuitively, this cold layer was more extreme in case 1 than in the other cases, even though the higher equivalence ratio in case 1 would result in an idealized injector momentum balance pointed further away from the inner wall than the momentum in case 2 and 3. In case 2 and 3, a hot recirculation zone formed in the corners near the injection plane, leaving the detonable mixture in a band in the center. However, in the third axis-normal plane (13 mm from injection) both cases start to show pockets of unmixed oxygen near the inner wall, some of which remains unburnt even at the exit plane of the chamber. Comparing the cold pockets with Fig. 2 reveals that much of the unburnt reactants in case 2 and 3 were colocated with the shear layer formed at the top of the traveling detonative structure.

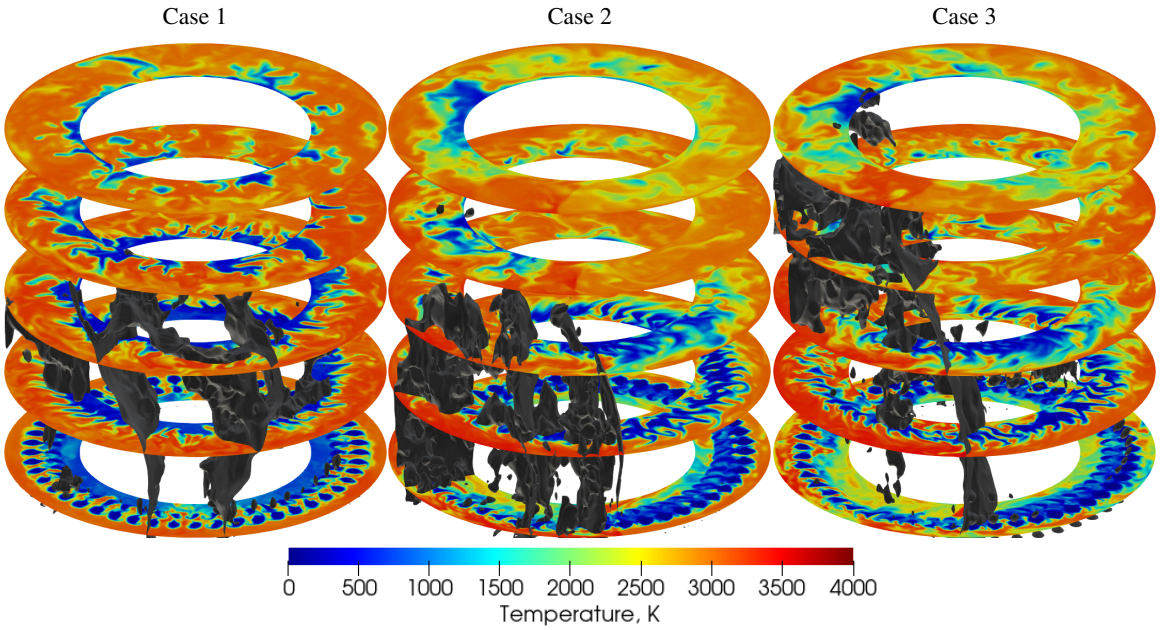

Figure 3: Isometric representation of temperature field in axis-normal slices, for the three simulations. 3D isocontour denotes 0.5 MPa.

4 Conclusions

Three simulations of a 25.4 mm RDRE were conducted, at varying flow conditions. An overall flow condition that operates with corotating waves in a previously-investigated 76.2 mm version of the engine was found to behave in a counterpropagating mode in the 25.4 mm design, operating with weaker waves. The change in operating behavior resulted in an inability for the 25.4 mm engine to fully burn all propellant, demonstrating that changes in dynamics caused by engine scale have important consequences on operating regime and performance.

It was also found that the 25.4 mm version of the engine exhibits the same double-shock structure that is characteristic of the 76.2 mm version of the engine. Although the leading part of the structure shock structure travels into unburnt propellant, the majority of the heat release corresponds to the later parts of the structure. It is still unclear what prevents the two-shock structure from coalescing during operation.

5 Acknowledgments

Preliminary work for these simulations was conducted by Dr. Christopher Lietz. This work has been supported by the Air Force Office of Scientific Research, under AFRL Lab Task 23RQCOR010 funded by the AFOSR Energy, Combustion, and Non-Equilibrium Thermodynamics portfolio, with Dr. Chiping Li as program manager. Additionally, the work was supported in part by high-performance computer time and resources from the DoD High Performance Computing Modernization Program. The views expressed are those of the authors, and do not necessarily reflect the official policy or position of the Department of the Air Force, the Department of Defense, or the U.S. Government.

References

[1] C. Knowlen, T. Mundt, and M. Kurosaka, "Experimental results for 25-mm and 51-mm rotating detonation rocket engine combustors," *Shock Waves*, vol. 33, no. 3, pp. 237–252, Apr. 2023.

[2] J. W. Bennewitz, J. R. Burr, B. R. Bigler, R. F. Burke, A. Lemcherfi, T. Mundt, T. Rezzag, E. W. Plaehn, J. Sosa, I. V. Walters, S. A. Schumaker, K. A. Ahmed, C. D. Slabaugh, C. Knowlen, and W. A. Hargus, "Experimental validation of rotating detonation for rocket propulsion," *Scientific Reports*, vol. 13, no. 1, p. 14204, Aug. 2023.

[3] M. Ross, A. P. Nair, A. Karagozian, R. M. Spearrin, and C. Lietz, "Synthetic Laser Measurements in Rotating Detonation Rocket Engine Simulations," in *AIAA SCITECH 2023 Forum*. National Harbor, MD & Online: American Institute of Aeronautics and Astronautics, Jan. 2023.

[4] M. Ross, J. R. Burr, and M. E. Harvazinski, "Relating High-Fidelity RDRE Simulations to Thermodynamic Cycles, Using Fluid Trajectories," in *AIAA SCITECH 2024 Forum*. Orlando, FL: American Institute of Aeronautics and Astronautics, Jan. 2024.

[5] W.-W. Kim and S. Menon, "An unsteady incompressible Navier–Stokes solver for large eddy simulation of turbulent flows," *International Journal for Numerical Methods in Fluids*, vol. 31, no. 6, pp. 983–1017, 1999.

[6] R. Maccormack, "The effect of viscosity in hypervelocity impact cratering," in *4th Aerodynamic Testing Conference*. Cincinnati,OH,U.S.A.: American Institute of Aeronautics and Astronautics, Apr. 1969.

[7] B. van Leer, "Towards the ultimate conservative difference scheme. V. A second-order sequel to Godunov's method," *Journal of Computational Physics*, vol. 32, no. 1, pp. 101–136, Jul. 1979.

[8] W.-W. Kim, S. Menon, W.-W. Kim, and S. Menon, "Application of the localized dynamic subgrid-scale model to turbulent wall-bounded flows," in *35th Aerospace Sciences Meeting and Exhibit*. Reno,NV,U.S.A.: American Institute of Aeronautics and Astronautics, Jan. 1997.

[9] R. Xu, S. S. Dammati, X. Shi, E. S. Genter, Z. Jozefik, M. E. Harvazinski, T. Lu, A. Y. Poludnenko, V. Sankaran, A. R. Kerstein, and H. Wang, "Modeling of high-speed, methane-air, turbulent combustion, Part II: Reduced methane oxidation chemistry," *Combustion and Flame*, vol. 263, p. 113380, May 2024.

[10] C. Lietz, Y. Desai, R. Munipalli, S. A. Schumaker, and V. Sankaran, "Flowfield analysis of a 3D simulation of a rotating detonation rocket engine," in *AIAA Scitech 2019 Forum*. San Diego, California: American Institute of Aeronautics and Astronautics, Jan. 2019.